HHS Public Access

Author manuscript

Science. Author manuscript; available in PMC 2017 May 23.

Published in final edited form as:

Science. 2016 April 29; 352(6285): 550–555. doi:10.1126/science.aad4821.

Changes in the composition of brain interstitial ions control the sleep - wake cycle

Fengfei Ding[1,†], **John O'Donnell**[1,†], **Qiwu Xu**[1], **Ning Kang**[1], **Nanna Goldman**[1], and **Maiken Nedergaard**[1,2,*]

[1]Center for Translational Neuromedicine, University of Rochester Medical Center, Rochester 14642, USA

[2]Center for Basic and Translational Neuroscience, Faculty of Health and Medical Sciences, University of Copenhagen, Copenhagen 2200, Denmark

Abstract

Wakefulness is driven by the widespread release of neuromodulators by the ascending arousal system. Yet, it is unclear how these substances orchestrate state-dependent, global changes in neuronal activity. Here we show that neuromodulators induce increases in the extracellular K^+ concentration ($[K^+]_e$) in cortical slices electrically silenced by tetrodotoxin. In vivo, arousal was linked to AMPA receptor-independent elevations of $[K^+]_e$ concomitant with decreases in $[Ca^{2+}]_e$, $[Mg^{2+}]_e$, $[H^+]_e$, and the extracellular volume. Opposite, natural sleep and anesthesia reduced $[K^+]_e$, while increasing $[Ca^{2+}]_e$, $[Mg^{2+}]_e$, $[H^+]_e$, as well as the extracellular volume. Local cortical activity of sleeping mice could be readily converted to the stereotypical EEG pattern of wakefulness by simply imposing a change in the extracellular ion composition. Thus, extracellular ions control the state-dependent patterns of neural activity.

Introduction

Wakefulness and sleep represent two fundamentally different behavioral states (1). While awake, we are responsive to our surroundings, integrate sensory input, recall memories, and make decisions, whereas contact with the outside world is limited during sleep. These two states of brain activity show characteristic patterns of cortical EEG, gene expression, and metabolic signature (2, 3). The concerted release of neuromodulators, including norepinephrine, acetylcholine, histamine, dopamine, and orexin mediates arousal (4). All of these neuromodulators individually alter the membrane properties, spiking activity, and intracellular signaling pathways of subpopulations of neurons and glia (5), but how they

*Corresponding author: nedergaard@urmc.rochester.edu.
†These authors contributed equally to this work.

Supplementary Materials
www.sciencemag.org
Materials and Methods
Figs. S1, S2, S3, S4, S5
Tables. S1
References (25–45)

implement the striking stereotypic patterns of EEG activity characterizing wakefulness versus sleep is not understood (6).

Neuronal excitability can be modulated by changes in the composition of extracellular ions. For example, moderate elevations of $[K^+]$ in the bath solution (1–2 mM) increase spontaneous and evoked excitatory activity in hippocampal slices, and more robust elevations (2–5 mM) trigger seizure-like activity (7). Lowering extracellular Ca^{2+} ($[Ca^{2+}]_e$) and extracellular Mg^{2+} ($[Mg^{2+}]_e$) also potently alters excitability (7).

Neuromodulators Increase Extracellular K+ Independently of Synaptic Activity

It is not known whether the changes in extracellular ion concentrations that occur during the natural sleep-wake cycle (8) are primary or secondary to alterations in electrical activity. In fact, the changes in extracellular ions that accompany behavioral states would be considered by most to be a consequence of different patterns of neuronal activity. However, ion transport is regulated by catecholamines outside the CNS (5). Here we asked whether neuromodulators also regulate ion transport in CNS and thereby the concentration of extracellular ions. We first recorded $[K^+]_e$ in cortical slices prepared from adult mice using K^+-sensitive microelectrodes (K^+-ISMs). Superfusion of a cocktail of neuromodulators at a concentration comparable to previous slice studies containing norepinephrine, acetylcholine, dopamine, orexin, and histamine triggered a rapid increase in $[K^+]_e$ averaging 0.43 ± 0.07 mM. Surprisingly, blocking neuronal activity by addition of TTX (1 μM) neither altered basal $[K^+]_e$ nor significantly suppressed the neuromodulator-cocktail induced $[K^+]_e$ increase, despite completely blocking spontaneous and evoked activity (Fig. 1). As a positive control, we inhibited energy metabolism by short-lasting exposure to the glycolytic inhibitor iodoacetate (10 mins 3.5 mM) - triggering an abrupt increase in $[K^+]_e$, which partly recovered during washout (Fig. 1F). As expected, TTX suppressed the increase in $[K^+]_e$ induced by inhibition of glycolysis (9). The insensitivity of neuromodulator induced $[K^+]_e$ elevations to TTX raises the question as to whether the concerted release of neuromodulators during arousal and wakefulness also drives an increase in $[K^+]_e$ in vivo, and if so, if this elevation is upstream of excitatory transmission or merely secondary to changes in local neuronal activity.

Wakefulness Triggers an Increase in Extracellular K+ that is Independent of AMPA Receptors

We next measured state-dependent changes in extracellular ion concentrations in vivo (Fig. S2A). All recordings were collected between zeitgeber times (ZT) 4 and 8 (ZT times are based on a 24 hour diurnal cycle standardized such that ZT0 is the beginning of the sleep period and ZT12 is the beginning of the awake period). Sleep was defined as periods with high ECoG delta activity and low EMG activity relative to periods where animals were awake. Starting from sleep, $[K^+]_e$ rose rapidly by 0.40 ± 0.05 mM (Fig. 2A and B) as animals awoke, before returning to baseline as animals fell back asleep. These transitions occurred quickly with increases peaking within 1.3 ± 0.02 s (range [0.1–8.6 s], $n = 27$

transitions), while the transition back to sleep was substantially slower and more variable, 13.9 ± 2.7 s (range [1.8–45.9 s], $t(55) = 3.22$, $P = 0.002$).

We next investigated the effect of isoflurane anesthesia on $[K^+]_e$ and collected recordings during the animals natural wake period (ZT16-20). After obtaining a stable awake $[K^+]_e$ baseline, 2% isoflurane was administered, which consistently triggered a sharp decrease in $[K^+]_e$ of 0.37 ± 0.06 mM (Fig. 2C). This decrease in $[K^+]_e$ remained stable throughout isoflurane administration and recovered to pre-anesthesia, awake levels over 148 ± 41 s following cessation of anesthesia ($n = 9$ animals). Both the shift into and recovery from anesthesia mirrored changes in ECoG and EMG activity (Fig. 2C).

To critically evaluate the stability of state-dependent ion shifts, microdialysis samples of the extracellular fluid were collected in freely behaving, unrestrained mice. The no-net flux paradigm was employed to estimate $[K^+]_e$, with 5 samples collected over several hours in which the $[K^+]$ in aCSF was stepwise altered (Fig. 2D). Estimates of $[K^+]_e$ were comparable to those recorded with K^+-ISMs in the cortex, 4.00 ± 0.17 mM versus 4.16 ± 0.09 mM in awake mice ($t(44) = 0.903$, $P = 0.371$, t-test). Microdialysis also showed a significant reduction in $[K^+]_e$ during sleep and isoflurane periods with values decreasing to 3.44 ± 0.11 mM in sleep, and 3.26 ± 0.12 mM in isoflurane (Fig. 2D).

To test whether state-dependent $[K^+]_e$ shifts are the result of changes in excitatory activity *in vivo*, we applied the AMPA receptor antagonist CNQX (200 μM). While CNQX potently and rapidly suppressed the ECoG power of awake mice, only a transient and short-lasting (<10 minutes) decrease in $[K^+]_e$ was observed, with $[K^+]_e$ returning to pre-CNQX concentrations despite continued suppression synaptic activity (Fig. S2B–C, F). Subsequent administration of isoflurane in the presence of CNQX decreased $[K^+]_e$ by 0.26 ± 0.02 mM (Fig. S2C). Thus, regulation of $[K^+]_e$ is dependent on state-modulation and not a direct measure of local glutamatergic activity. State-dependent transitions in brain activity are also linked to changes in the extracellular space volume (10). As the Na^+/K^+-ATPase is the chief regulator of both $[K^+]_e$ and cell volume (7) we asked if the decreased $[K^+]_e$ in response to isoflurane anesthesia is linked to expanded extracellular space. Despite markedly reducing ECoG power throughout recordings, CNQX neither changed awake extracellular space nor inhibited isoflurane-induced expansion (Fig. S2E). This indicates that local synaptic transmission (ECoG power) is not the primary determinant of state-dependent changes of either $[K^+]_e$ or the extracellular space volume.

Together, cortical recordings of $[K^+]_e$ as well as sampling of the extracellular fluid by microdialysis showed consistent decreases in $[K^+]_e$ as animals transitioned from the awake state to sleep. Blocking local synaptic transmission with CNQX did not affect state-dependent changes in $[K^+]_e$ (Fig. 2E).

Extracellular Ca^{2+} Decreases During Wakefulness

Are cortical extracellular Ca^{2+} concentrations also regulated by the sleep-wake cycle? Opposite to the rise in $[K^+]_e$, $[Ca^{2+}]_e$ consistently decreased 0.13 ± 0.02 mM as mice transitioned from sleep to awake states and, conversely, increased by 0.11 ± 0.01 mM as the

mice returned to sleep (Fig. 3A and B). These state-dependent $[Ca^{2+}]_e$ shifts were slow compared to $[K^+]_e$, with sleep-to-awake transitions taking 51.5 ± 8.8 s ([4.5–156.0 s], t-test $[Ca^{2+}]_e$ versus $[K^+]_e$: t(*20*) = 5.379, $P < 0.0001$) and awake-to-sleep occurring over 63.3 ± 8.9 s ([19.3–116.1 s], t-test $[Ca^{2+}]_e$ versus $[K^+]_e$: t(*16*) = 6.696, $P < 0.0001$). Isoflurane administered to awake mice drove a slow increase in $[Ca^{2+}]_e$ throughout the duration of anesthesia, with levels rising by 0.26 ± 0.02 mM (Fig. 3C). This rise in $[Ca^{2+}]_e$ continued throughout and past the cessation of anesthesia, peaking at 1.2 ± 1.6 min ([−6.2 to 12.4 min], $n = 11$ animals), and taking 22.6 ± 4.8 min ([4.3 – 49.2 min], $n = 10$ animals) to recover.

Microdialysis was used to assess the stability of state-dependent $[Ca^{2+}]_e$ shifts using the no-net flux method. Due to the slow time-course of $[Ca^{2+}]_e$ transitions and short awakenings associated with sample collection, we pooled sleep and awake samples and compared them to isoflurane, finding that $[Ca^{2+}]_e$ increases by 0.25 ± 0.08 mM under isoflurane anesthesia (Fig. 3D); comparable to *in vivo* $[Ca^{2+}]_e$ isoflurane recordings (Fig. 3E).

CNQX suppressed ECoG power by >60%, but did not significantly alter awake $[Ca^{2+}]_e$ or isoflurane-induced $[Ca^{2+}]_e$ increases (Fig. 3E), indicating that local glutamatergic activity did not control the shifts in $[Ca^{2+}]_e$. Together, all shifts from awake to isoflurane anesthetized states showed surprising consistency (Fig. 3E). However, state-dependent changes in $[Ca^{2+}]_e$ could be secondary to shifts in $[K^+]_e$. We therefore increased $[K^+]_e$ in the aCSF covering the cranial window from 2.8 to 4.5 mM, increasing $[K^+]_e$ 200 μm below the pial surface by 0.47 ± 0.07 mM (t-test: $t(7) = 6.861$, $P < 0.0001$). However, imposing this increase in $[K^+]_e$ had no detectable effect on the local $[Ca^{2+}]_e$ concentration suggesting that $[Ca^{2+}]_e$ changes are not secondary to state-dependent $[K^+]_e$ changes (paired t-test: $t(2) = 0.855$, $P = 0.483$).

Extracellular Mg^{2+} is Low During Wakefulness and Increases During Sleep and Anesthesia

In sleep and awake states, minor but consistent shifts in free $[Mg^{2+}]_e$ were identified, with $[Mg^{2+}]_e$ decreasing by 0.11 ± 0.01 mM (Fig. 4A) as mice transitioned from sleep to awake, and increasing again by 0.13 ± 0.02 mM (Fig. 4B) as animals were observed to return to sleep. Transitions occurred slowly from both sleep to awake (68.9 ± 8.8 s; [5–342 s]; $n = 55$ transitions) and awake to sleep (141.1 ± 14.8 s; [15.1–470 s]; $n = 49$ transitions). Isoflurane anesthesia also increased $[Mg^{2+}]_e$ by 0.44 ± 0.07 mM in awake mice (Fig. 4C) before gradually returning to baseline over 26.7 ± 5.7 min ([9.6–66.3 min] $n = 9$ animals) following the cessation of anesthesia.

Microdialysis samples were collected during the sleep (ZT2-8) and awake (ZT14-20) periods, and were pooled and compared with isoflurane-induced shifts in $[Mg^{2+}]_e$, demonstrating an increase of 0.32 ± 0.13 mM $[Mg^{2+}]_e$ in isoflurane samples (Fig. 4D). CNQX neither altered basal $[Mg^{2+}]_e$ nor the previously observed isoflurane-induced increase in $[Mg^{2+}]_e$ (Fig. 4E). Thus, across all experiments, $[Mg^{2+}]_e$ increased as mice went from awake to sleep or isoflurane (Fig. 4E).

Robust changes in pH were also noted with isoflurane anesthesia. Recordings with pH-sensitive microelectrodes showed that pH decreased from an awake level of 7.39 ± 0.03 to a stable isoflurane-anesthetized level of 7.26 ± 0.02 (Fig. S3).

Local Manipulation of Extracellular Ions Controls Neuronal Activity and Extracellular Space Volume

Can interstitial ion composition be locally altered to mimic natural sleep or awake concentrations? Because ions in the aCSF covering the cranial window continuously exchange with those in the interstitial fluid, we formulated awake-inducing and sleep-inducing aCSFs (table S1) to drive local cortex to the ionic composition of the state opposite the overarching behavioral state (Fig. S4). In sleeping mice (ZT4-8), the awake-inducing aCSF increased $[K^+]_e$ by 0.47 ± 0.07 mM (versus 0.37 ± 0.06 mM in awake to isoflurane transitions), decrease $[Ca^{2+}]_e$ by 0.31 ± 0.06 mM (versus 0.26 ± 0.02 mM), decrease $[Mg^{2+}]_e$ by 0.35 ± 0.02 mM (versus 0.44 ± 0.07 mM). Sleep-inducing aCSF applied to cortex of awake mice (ZT16-20) resulted in similar shifts, though in the opposite direction. Thus, both solutions could elicit local changes in $[K^+]_e$, $[Ca^{2+}]_e$, and $[Mg^{2+}]_e$ comparable to those seen in transitions from awake to isoflurane anesthesia (Fig. S4B and D). Only pH showed a significantly smaller amplitude shift than those observed in awake to isoflurane state transitions, likely reflecting the efficacy by which CO_2/HCO_3^- system buffer pH (Fig. S4B and D) (7).

Can local manipulation of extracellular ions in itself drive sleep or awake-like patterns of neuronal activity? We prepared mice with two separate cranial windows located over the left and right hemisphere and recorded ECoG symmetrically from each (Fig. 5A). Starting in sleeping mice (ZT4-8) with sleep aCSF (table S1) over each window, recordings were collected from each hemisphere. Following this baseline period, the aCSF over the left window was removed and replaced with awake-inducing aCSF. When activity in the left hemisphere was normalized to the right to preclude changes from global state transitions, we observed a 34 ± 5% decrease in 1–4 Hz ECoG power following application of awake-inducing aCSF, with no change in activity in the contralateral hemisphere (Fig. 5B). In comparison natural sleep-to-wake transitions, decreases the 1–4 Hz power by 31.1 ± 3.1% (mean ± SEM of all data, $n = 128$ transitions). Conversely, could sleep-inducing aCSF increase local delta power in awake mice? Recording between ZT16-20, awake mice were prepared with awake aCSF covering each cranial window. After a baseline recording, the aCSF over the left hemisphere was replaced with sleep-inducing aCSF, resulting in a 43 ± 13% relative increase in 1–4 Hz delta power in the left hemisphere exposed to the sleep-inducing aCSF (Fig. 5C).

Because state-dependent changes in brain activity are also linked to marked changes in the extracellular space volume (10), we asked whether altering the local ion composition can drive extracellular space volume changes. TMA^+ recordings showed that in lightly-anesthetized mice (1% isoflurane administered to avoid arousal episodes), changing aCSF from sleep aCSF to awake-inducing induced a 21.7 ± 1.2% decrease in the local extracellular space volume (Fig. 5D). Tortuosity (λ) was consistent with previous studies

(11). Conversely, the extracellular space volume increased by 32.2 ± 2.9% from baseline recordings obtained with awake aCSF to those recorded using sleep-inducing aCSF in awake mice, despite mice remaining awake and mobile, with tortuosity remaining unchanged (Fig. 5D).

Brain-Wide Manipulations of Extracellular Ions Can Override Behavioral States

Would global manipulation of the extracellular ion composition be sufficient to change the behavioral state of mice? We implanted EEG and EMG electrodes, as well as a cannula in cisterna magna (10). In sleeping mice (ZT4), a baseline recording was acquired infusing sleep aCSF followed by a switch to a modified awake-inducing aCSF (Fig. 5E). This switch triggered a robust change in EEG/EMG activity (Fig. 5E), with decreased EEG amplitude and delta prevalence and increased EMG activity, indicative of an awake-phenotype. Infusion rates were comparable to CSF production, and ion concentrations were chosen to account for total brain and CSF volume (supplementary methods). Typically aCSF infusion itself did not alter EEG activity (Fig. S5A–B). Mice returned to sleep shortly following discontinuation of awake-inducing aCSF infusion (Fig. 5F). We next tested whether infusion of a modified sleep-inducing aCSF could alter the behavioral state of mice during their awake-period. Baseline EEG/EMG activity characteristic of awake mice was recorded while infusing awake aCSF followed by a modified sleep-inducing aCSF. Infusion induced a sharp reduction in EMG activity coupled to a marked increase in slow-wave EEG activity, indicating a shift toward sleep. EEG/EMG activity typical of wakefulness rapidly recovered upon stopping infusion of the modified sleep-inducing aCSF (Fig. 5G).

Discussion

Understanding what drives arousal is essential for deciphering key aspects of consciousness and the lack thereof during sleep and anesthesia. We found that the transition from wakefulness to sleep is accompanied by a marked and sustained change in the concentration of key extracellular ions and the volume of the extracellular space. Arousal triggers a rapid rise in $[K^+]_e$, combined with a decrease in $[Ca^{2+}]_e$, $[Mg^{2+}]_e$, $[H^+]_e$, and a shrinkage of extracellular space. Natural sleep or anesthesia induces the inverse changes in extracellular ion concentrations, and is accompanied by an expansion of extracellular space volume. State-dependent shifts in $[K^+]_e$ occurred within seconds, whereas the changes in $[Ca^{2+}]_e$ and $[Mg^{2+}]_e$ were slow, taking 51.5 ± 8.8 s and 68.9 ± 8.8 s, respectively, for sleep to awake transitions. Extracellular fluid samples by microdialysis confirmed and extended the *in vivo* recordings by documenting that state-dependent differences in extracellular $[K^+]_e$, $[Ca^{2+}]_e$, and $[Mg^{2+}]_e$ concentrations persisted over prolonged period of hours in freely behaving animals (Figs. 2–4). Microdialysis experiments suggested that state-dependent changes in extracellular ions included widespread cortical areas since the samples were collected by 2 mm long probes.

All ions exhibited far more consistent, rapid transitions during arousal relative to falling asleep. This is consistent with the need to quickly shift from sleep to awake states when presented with novel, threatening, or unexpected stimuli, and with the overarching ability of

brainstem neuromodulatory centers to drive near-immediate responses to behaviorally relevant events (12). Relative to $[K^+]_e$, the 5-fold slower transition of $[Ca^{2+}]_e$ and $[Mg^{2+}]_e$ may reflect differences in the transport or buffering of these ions, and suggests that beyond the immediate capacity of neuromodulators to drive quick arousal, it takes longer for composition of interstitial ions to fully stabilize. $[Ca^{2+}]_e$ and $[Mg^{2+}]_e$ exhibited very slow recoveries following anesthesia often lasting 10–30 min. Interestingly, ions appeared to exhibit larger shifts in the immediate post-induction and recovery period. This biphasic activity may suggest a complex shift in neuromodulatory activity during these anesthetic transitions, and, with $[Ca^{2+}]_e$ and $[Mg^{2+}]_e$ taking much longer than $[K^+]_e$ to return to a stable awake concentration, may relate to the confusion and post-operative delirium that follows general anesthesia. In fact, high levels of serum $[Ca^{2+}]_e$ and $[Mg^{2+}]_e$ can manifest as subacute delirium (7).

Perhaps the most interesting observation is the state-dependent change in $[Mg^{2+}]_e$. Previous studies have shown that $[Mg^{2+}]_e$ in CNS is in the range of ~0.8–1.2 mM or slightly lower than in plasma (13, 14), but $[Mg^{2+}]_e$ homeostasis has received little attention (15). In electrophysiological studies, manipulation of $[Mg^{2+}]_e$ is commonly employed, because low $[Mg^{2+}]_e$ relieves the depolarization block of the N-methyl-D-aspartate (NMDA) receptors and facilitates induction of LTP and, in more extreme cases, seizure (7, 16). Interestingly, wakefulness and sleep deprivation are linked to upregulation of pathways downstream of NMDA receptor activation, including CamKII, ERK, and pCreb (1, 17). The decline in $[Mg^{2+}]_e$ during wakefulness may thereby, in combination with membrane depolarization induced by the elevation of $[K^+]_e$, contribute to the gene expression pattern characteristic of wakefulness. The finding that $[Mg^{2+}]_e$ increases during sleep is consistent with the observation that changes in dietary magnesium can have a profound impact on learning and memory, possibly by improving both the amount and quality of sleep (18, 19).

Arousal is triggered by the concerted activity of neurons located in brainstem, hypothalamus, and basal forebrain (1, 4). Projections from these clusters of neurons release norepinephrine, acetylcholine, orexin, serotonin, dopamine, and histamine over widespread areas of CNS (12). Considerable redundancy exists in the system, since acute antagonism, ablation, or activation has documented the importance of the individual components in regulating arousal, but such perturbations rarely produce long-term effects (12). An unanswered question is how these neuromodulators drive global changes in EEG activity. Conventional thinking is that the neuromodulators alter the membrane properties and spiking activity of select subtypes of neurons (5). Our findings show that a parallel path exists: A cocktail of neuromodulators consistently increased $[K^+]_e$ in cortical slices and TTX did not significantly suppress the $[K^+]_e$ increase, suggesting that this shift is not merely a consequence of local synaptic activity. In vivo, inhibition of AMPA receptors only transiently reduced $[K^+]_e$, with levels returning to baseline in <10 minutes despite continued suppression of ECoG activity by >60% (Figs. 2E and S2). This response to an external challenge suggests that ionic homeostasis is a tightly regulated in a state-dependent, neuronal-activity independent manner. Based on this, we propose that the neuromodulators, in addition to their well-documented, direct effect on neuronal activity, maintain sleep and awake states by creating a state-dependent set-point for interstitial ion concentrations that stabilize over seconds-to-minutes; minimizing changes resulting from transient burst firing

or suppression of these brainstem nuclei. In sleep and anesthesia, lower concentrations of $[K^+]_e$ will tend to hyperpolarize neurons, with high $[Ca^{2+}]_e$ and $[Mg^{2+}]_e$ enhancing this effect through surface charge screening and inactivation of the NALCN channel-dependent Na^+-leak current (20). High $[Mg^{2+}]_e$ in combination with hyperpolarization will reduce the likelihood of NMDA receptor activation during sleep, reducing the brain's ability to undergo activity-dependent changes in excitatory transmission (LTP). Manipulation of $[K^+]_e$, $[Ca^{2+}]_e$, and $[Mg^{2+}]_e$ in the CSF bathing the brain drove behavioral shifts between sleep and awake states (Fig. 5). Interestingly, astrocytic Ca^{2+} signaling is also enhanced by lowering of $[Ca^{2+}]_e$ and $[Mg^{2+}]_e$ (21–23), and is strongly inhibited by anesthesia (24). These observations suggest that regulation of extracellular ion homeostasis is sufficient to alter behavioral state both locally and globally, providing a path for neuromodulators to exert consistent, stable shifts in neuronal and astrocytic activity across the brain.

A myriad of electrophysiological slice studies have in the past taken advantage of minor modifications in the ion composition of the bath solution to induce stable and highly reproducible changes in neural excitability. The observations presented here suggest that the CNS itself employs the same trick to control state-dependent changes in neuronal activity. One advantage of this "ionostatic control" of neural activity is to provide a backdrop for coordinating shifts in behavioral state through the widespread regulation of excitability without relying on complex receptor activation in diverse subclasses of neurons. The characteristic state-dependent pattern of EEG activity can, at least in part, be explained by differences in extracellular ion composition in sleep versus wakefulness. Our observations add new and critical insight into understanding what drives arousal, as well as the loss of consciousness during sleep and anesthesia. Future studies should define whether changes in extracellular ion concentrations are involved in disorders such as stupor and coma.

Supplementary Material

Refer to Web version on PubMed Central for supplementary material.

Acknowledgments

This study was supported by NIH (NS078167 and NS078304) and Office of Naval Research. We thank Wei Song, Rune Rasmussen, Eric Nicholas, and Weiguo Peng, for expert technical assistance and Chiara Cirelli, Giulio Tononi, and Charles Nicholson for comments on the manuscript. All authors contributed to data collection, technical design and writing.

References and Notes

1. Tononi G, Cirelli C. Sleep and the price of plasticity: from synaptic and cellular homeostasis to memory consolidation and integration. Neuron. 2014; 81:12–34. [PubMed: 24411729]
2. Benington JH, Heller HC. Restoration of brain energy metabolism as the function of sleep. Prog Neurobiol. 1995; 45:347–360. [PubMed: 7624482]
3. Hinard V, et al. Key electrophysiological, molecular, and metabolic signatures of sleep and wakefulness revealed in primary cortical cultures. J Neurosci. 2012; 32:12506–12517. [PubMed: 22956841]
4. Saper CB, Scammell TE, Lu J. Hypothalamic regulation of sleep and circadian rhythms. Nature. 2005; 437:1257–1263. [PubMed: 16251950]

5. O'Donnell J, Zeppenfeld D, McConnell E, Pena S, Nedergaard M. Norepinephrine: a neuromodulator that boosts the function of multiple cell types to optimize CNS performance. Neurochem Res. 2012; 37:2496–2512. [PubMed: 22717696]
6. Steriade M, McCormick DA, Sejnowski TJ. Thalamocortical oscillations in the sleeping and aroused brain. Science. 1993; 262:679–685. [PubMed: 8235588]
7. Somjen, GG. Ions in the brain : normal function, seizures, and stroke. Oxford University Press; Oxford ; New York: 2004. p. xxixp. 470
8. Seigneur J, Kroeger D, Nita DA, Amzica F. Cholinergic action on cortical glial cells in vivo. Cereb Cortex. 2006; 16:655–668. [PubMed: 16093563]
9. Rothman SM. Synaptic activity mediates death of hypoxic neurons. Science. 1983; 220:536–537. [PubMed: 6836300]
10. Xie L, et al. Sleep drives metabolite clearance from the adult brain. Science. 2013; 342:373–377. [PubMed: 24136970]
11. Anderova M, et al. Effect of elevated K(+), hypotonic stress, and cortical spreading depression on astrocyte swelling in GFAP-deficient mice. Glia. 2001; 35:189–203. [PubMed: 11494410]
12. Saper CB, Fuller PM, Pedersen NP, Lu J, Scammell TE. Sleep state switching. Neuron. 2010; 68:1023–1042. [PubMed: 21172606]
13. Hansen AJ. Effect of anoxia on ion distribution in the brain. Physiol Rev. 1985; 65:101–148. [PubMed: 3880896]
14. Sun L, et al. Magnesium concentration in the cerebrospinal fluid of mice and its response to changes in serum magnesium concentration. Magnes Res. 2009; 22:266–272. [PubMed: 20228005]
15. Romani AM. Cellular magnesium homeostasis. Arch Biochem Biophys. 2011; 512:1–23. [PubMed: 21640700]
16. Anderson WW, Lewis DV, Swartzwelder HS, Wilson WA. Magnesium-free medium activates seizure-like events in the rat hippocampal slice. Brain Res. 1986; 398:215–219. [PubMed: 3801897]
17. Gilestro GF, Tononi G, Cirelli C. Widespread changes in synaptic markers as a function of sleep and wakefulness in Drosophila. Science. 2009; 324:109–112. [PubMed: 19342593]
18. Abbasi B, et al. The effect of magnesium supplementation on primary insomnia in elderly: A double-blind placebo-controlled clinical trial. J Res Med Sci. 2012; 17:1161–1169. [PubMed: 23853635]
19. Slutsky I, et al. Enhancement of learning and memory by elevating brain magnesium. Neuron. 2010; 65:165–177. [PubMed: 20152124]
20. Lu B, et al. Extracellular calcium controls background current and neuronal excitability via an UNC79-UNC80-NALCN cation channel complex. Neuron. 2010; 68:488–499. [PubMed: 21040849]
21. Schummers J, Yu H, Sur M. Tuned responses of astrocytes and their influence on hemodynamic signals in the visual cortex. Science. 2008; 320:1638–1643. [PubMed: 18566287]
22. Sontheimer H. Voltage-dependent ion channels in glial cells. Glia. 1994; 11:156–172. [PubMed: 7523291]
23. Torres A, et al. Extracellular Ca(2)(+) acts as a mediator of communication from neurons to glia. Sci Signal. 2012; 5:ra8. [PubMed: 22275221]
24. Thrane AS, et al. General anesthesia selectively disrupts astrocyte calcium signaling in the awake mouse cortex. Proc Natl Acad Sci U S A. 2012; 109:18974–18979. [PubMed: 23112168]
25. Wang F, et al. Astrocytes modulate neural network activity by Ca(2)+-dependent uptake of extracellular K+ Sci Signal. 2012; 5:ra26. [PubMed: 22472648]
26. Chesler M, Chen JC, Kraig RP. Determination of extracellular bicarbonate and carbon dioxide concentrations in brain slices using carbonate and pH-selective microelectrodes. J Neurosci Methods. 1994; 53:129–136. [PubMed: 7823615]
27. Schaller U, Spichiger UE, Simon W. Novel magnesium ion-selective microelectrodes based on a neutral carrier. Pflugers Arch. 1993; 423:338–342. [PubMed: 8321635]

28. Nicholson C. Ion-selective microelectrodes and diffusion measurements as tools to explore the brain cell microenvironment. J Neurosci Methods. 1993; 48:199–213. [PubMed: 8412303]
29. Umezawa Y, Umezawa K, Sato H. Selectivity Coefficients for Ion-Selective Electrodes: Recommended Methods for Reporting $K^{Pot}_{A,B}$ Values. Pure & Appl Che. 1995; 57:507–518.
30. Cotrina ML, et al. Astrocytic gap junctions remain open during ischemic conditions. J Neurosci. 1998; 18:2520–2537. [PubMed: 9502812]
31. Bickler PE, Kelleher JA. Fructose-1,6-bisphosphate stabilizes brain intracellular calcium during hypoxia in rats. Stroke. 1992; 23:1617–1622. [PubMed: 1440710]
32. Rangroo Thrane V, et al. Ammonia triggers neuronal disinhibition and seizures by impairing astrocyte potassium buffering. Nat Med. 2013; 19:1643–1648. [PubMed: 24240184]
33. Tian GF, et al. An astrocytic basis of epilepsy. Nat Med. 2005; 11:973–981. [PubMed: 16116433]
34. Kress BT, et al. Impairment of paravascular clearance pathways in the aging brain. Ann Neurol. 2014; 76:845–861. [PubMed: 25204284]
35. Nicholson C. Quantitative analysis of extracellular space using the method of TMA+ iontophoresis and the issue of TMA+ uptake. Can J Physiol Pharmacol. 1992; 70(Suppl):S314–322. [PubMed: 1295682]
36. Chvatal A, et al. Changes in glial K+ currents with decreased extracellular volume in developing rat white matter. J Neurosci Res. 1997; 49:98–106. [PubMed: 9211994]
37. Sykova E, et al. Changes in extracellular space size and geometry in APP23 transgenic mice: a model of Alzheimer's disease. Proc Natl Acad Sci U S A. 2005; 102:479–484. [PubMed: 15630088]
38. Veasey SC, et al. An automated system for recording and analysis of sleep in mice. Sleep. 2000; 23:1025–1040. [PubMed: 11145318]
39. Naylor E, et al. The circadian clock mutation alters sleep homeostasis in the mouse. J Neurosci. 2000; 20:8138–8143. [PubMed: 11050136]
40. Oshio K, Watanabe H, Song Y, Verkman AS, Manley GT. Reduced cerebrospinal fluid production and intracranial pressure in mice lacking choroid plexus water channel Aquaporin-1. FASEB J. 2005; 19:76–78. [PubMed: 15533949]
41. Roderick TH, Wimer RE, Wimer CC, Schwartzkroin PA. Genetic and phenotypic variation in weight of brain and spinal cord between inbred strains of mice. Brain Res. 1973; 64:345–353. [PubMed: 4781345]
42. Moazen M, et al. Intracranial pressure changes during mouse development. J Biomech. 2015
43. Kimelberg HK, Nedergaard M. Functions of astrocytes and their potential as therapeutic targets. Neurotherapeutics. 2010; 7:338–353. [PubMed: 20880499]
44. Jones SR, et al. Profound neuronal plasticity in response to inactivation of the dopamine transporter. Proc Natl Acad Sci U S A. 1998; 95:4029–4034. [PubMed: 9520487]
45. Martinez-Valverde T, et al. Brain microdialysis as a tool to explore the ionic profile of the brain extracellular space in neurocritical patients: a methodological approach and feasibility study. J Neurotrauma. 2015; 32:7–16. [PubMed: 25019674]

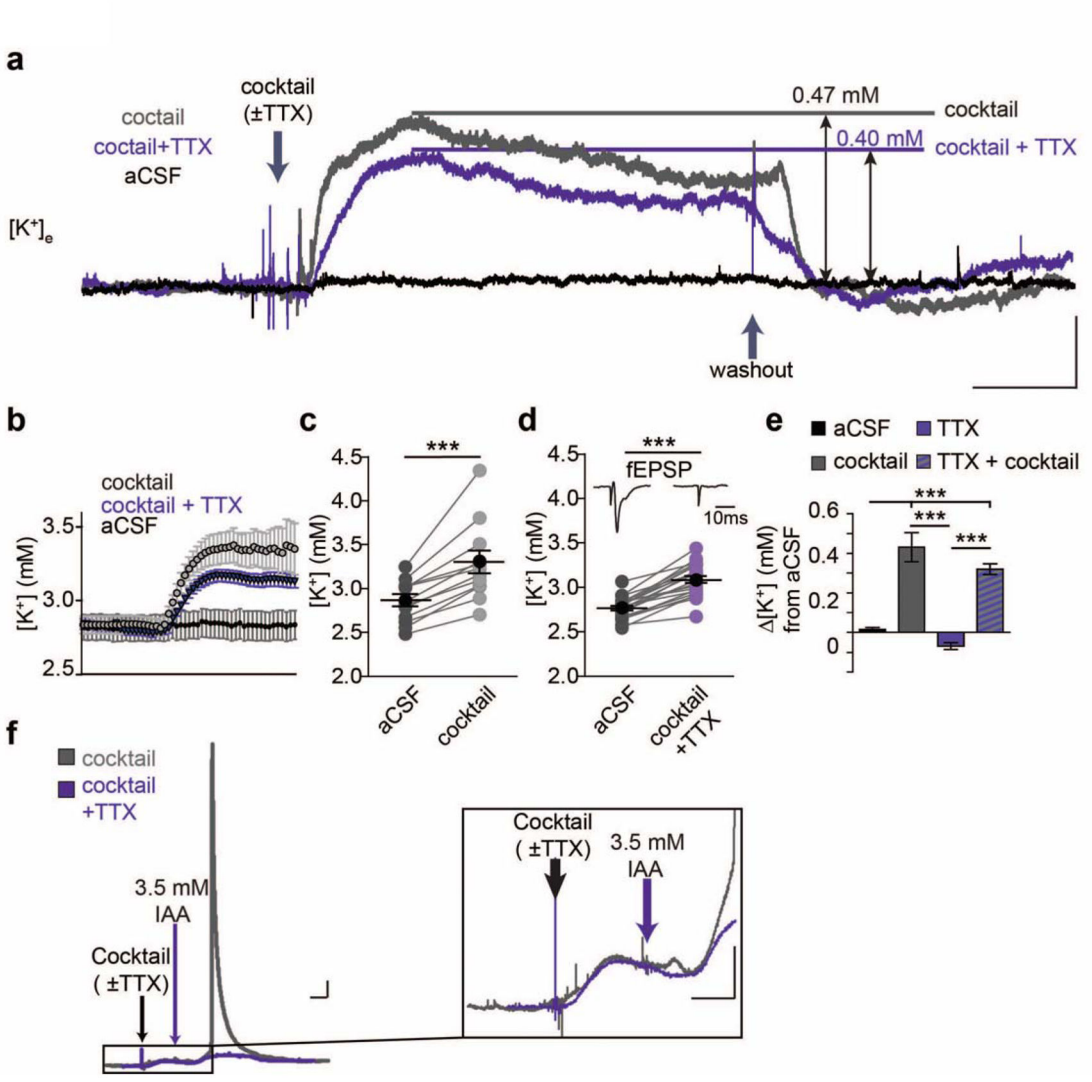

Fig. 1.

Neuromodulators increase $[K^+]_e$ concentration in the absence of neuronal activity. (**A**) Representative traces of $[K^+]_e$ shifts before, during, and after administering the neuromodulator cocktail. Scale bar: x = 5 min, y = 0.2 mM $[K^+]_e$ (**B**) 30 s binned averages of shifts before and after neuromodulator cocktail (**C** and **D**) Summary of $[K^+]_e$ increase following neuromodulator cocktail application in slices ± TTX (paired t-test, **C** (-TTX): $t(11) = 5.871$, $P = 0.0001$; **D** (+TTX), $t(21) = 11.69$, $P < 0.0001$). Inset: representative fEPSP recordings before and after application of TTX. Scale bar = 10 ms (**E**) Summarized shifts at 10 minutes following changing perfusion solution. $n = 6$ (cocktail-free aCSF), 12 (cocktail), 10 (aCSF+TTX), 22 (cocktail+TTX). One-way ANOVA: $F(3,46) = 25.94$, $P < 0.0001$. Post-hoc Tukey test: ** $P < 0.01$, *** $P < 0.001$. (**F**) Representative trace of large $[K^+]_e$ spike following metabolic stress using iodoacetate (IA). Trace includes pre-cocktail baseline, aCSF + cocktail, aCSF + IA and return to baseline aCSF. (*Right*) Magnified trace showing $[K^+]_e$ increases in slices treated with the neuromodulator cocktail (±TTX) followed by IA. Scale bars: x = 5 min, y = 0.2 mM $[K^+]_e$. Mean (black circle) ± SEM.

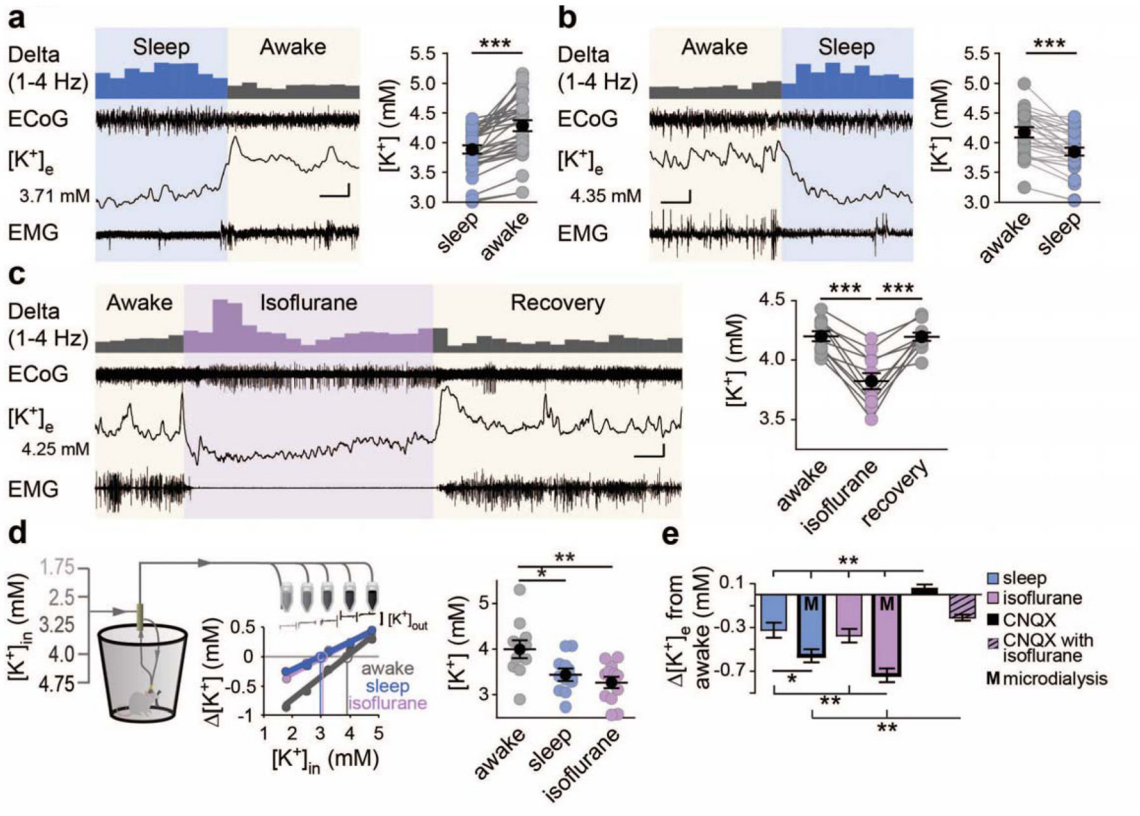

Fig. 2.

Extracellular K^+ is higher during wakefulness. (**A** and **B**) Representative ECoG, $[K^+]_e$, and EMG recordings with a data summary of state transitions in sleep to awake (**A**) or awake to sleep (**B**) Initial $[K^+]_e$ concentrations are shown to the left, and the 1–4 Hz power is displayed above to illustrate state-dependent shifts, binned at 10 s for clarity. $n = 34$ transitions; One-way, repeated measures ANOVA: $F(3,99) = 9.536$, $P < 0.0001$. Tukey post-hoc multiple comparisons test: $^{***}P < 0.001$. Scale bar: x = 20 s, y = 0.1 mM $[K^+]_e$; ECoG = 0.75 mV; EMG = 0.3 mV (**A**), 1 mV (**B**). (**C**) Representative recording of awake to isoflurane transitions recorded during the natural awake period (ZT16-20). $n = 11$ animals. One-way repeated measures ANOVA: $F(2,20) = 35.61$, $P < 0.0001$. Post-hoc Tukey test: $^{***}P < 0.001$. Scale bar: x = 1.5 min, y = 0.15 mM $[K^+]_e$, 0.75 mV EMG and ECoG. (**D**) Microdialysis samples collected from freely moving mice during their awake (ZT14-20) or sleeping (ZT2-8) period, and under isoflurane anesthesia. (*Left*) Schematic illustrating setup and inflow $[K^+]$ gradient with representative ISM trace and sample no-net flux method plot used for $[K^+]_e$ estimate. (right) Summary of $[K^+]_e$ by state: $n = 12$ awake, 12 sleep, and 13 isoflurane animals. One-way ANOVA: $F(2, 34) = 8.055$, $P = 0.0014$. Post-hoc Tukey test: $^{*}P < 0.05$, $^{**}P < 0.01$. (**E**) Comparison of all state-dependent transitions. One-way ANOVA comparing mean shifts by group: $F(5,161) = 16.61$, $P < 0.0001$. Post-hoc Tukey test: $^{*}P < 0.05$, $^{**}P < 0.01$. Mean (black circle) ± SEM

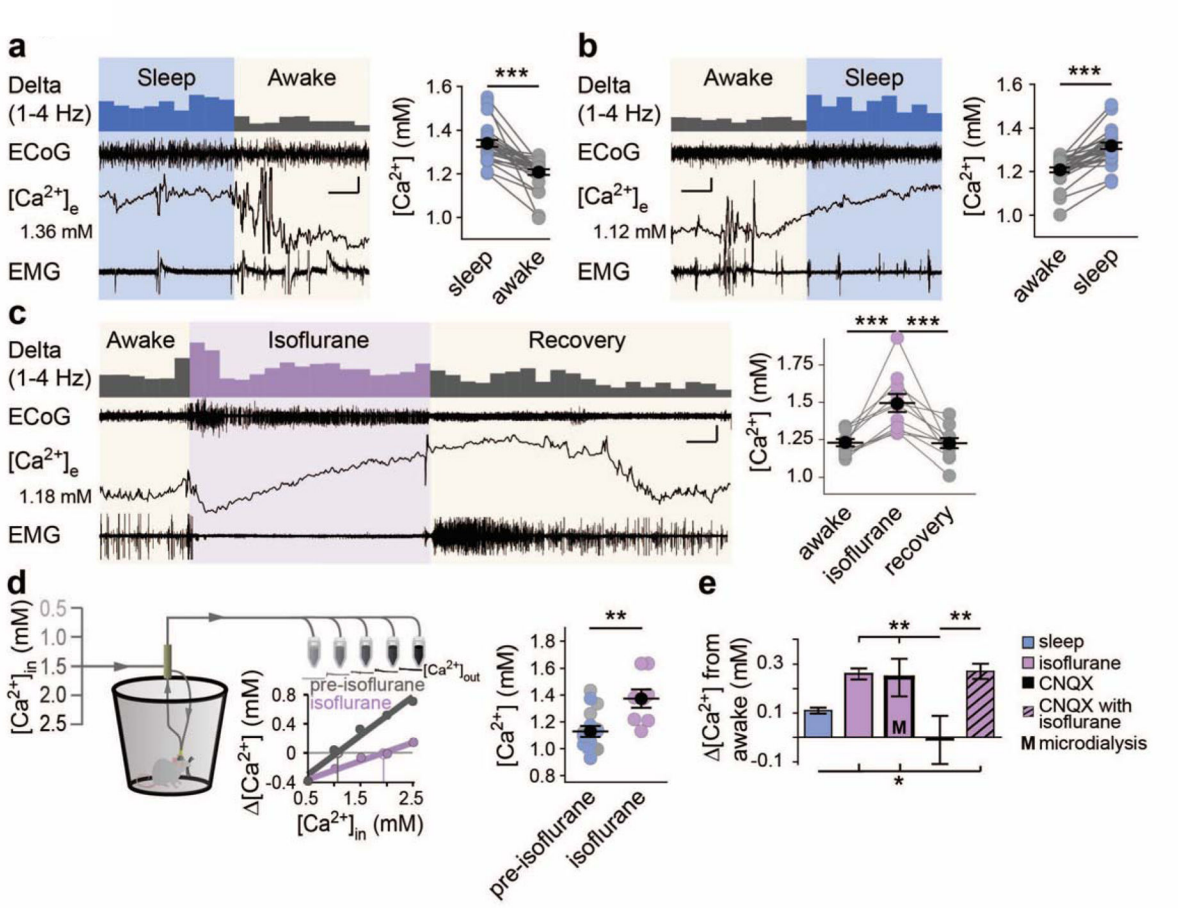

Fig. 3.

Extracellular Ca^{2+} decreases during wakefulness. (**A** and **B**) Representative ECoG, EMG, and $[Ca^{2+}]_e$ recordings in sleep to awake (**A**) and awake to sleep (**B**). Initial $[Ca^{2+}]_e$ is listed to the left with 1–4 Hz power presented above. $n = 28$ transitions. One-way, repeated measures ANOVA: F(3,81) = 39.91, $P < 0.0001$. Post-hoc Tukey test: ***$P < 0.001$. Scale bars: x = 20 s (**A**), 40 s (**B**), y: $[Ca^{2+}]_e$ = 0.05 mM, 0.75 mV EMG/ECoG (**C**) Representative recording of isoflurane induction and recovery (ZT16-20) and data summary. $n = 11$ animals. One-way repeated measures ANOVA: F(2,20) = 18.52, $P < 0.0001$. Post-hoc Tukey test: ***$P < 0.001$. Scale bar: x = 6 min, y = $[Ca^{2+}]_e$ = 0.2 mM, 0.5 mV EMG/ECoG. (**D**) Schematic of microdialysis collection. Individual sleep (light blue) and awake (gray) data are pooled and compared to isoflurane. $n = 8$ awake, 8 sleep, and 8 isoflurane. Two-tailed t-test of isoflurane versus non isoflurane: $t(22) = 3.420$, $P = 0.003$. **$P < 0.01$. (**E**) Comparisons of $[Ca^{2+}]_e$ shifts from the *awake* to sleep, isoflurane, CNQX and CNQX + isoflurane. $n = 8$ animals CNQX and CNQX + Isoflurane One-way ANOVA comparison of state-dependent shifts: F(4,117) = 5.824, $P = 0.0003$; Post-hoc Tukey test: *$P < 0.05$, **$P < 0.01$. Mean (black circle) ± SEM.

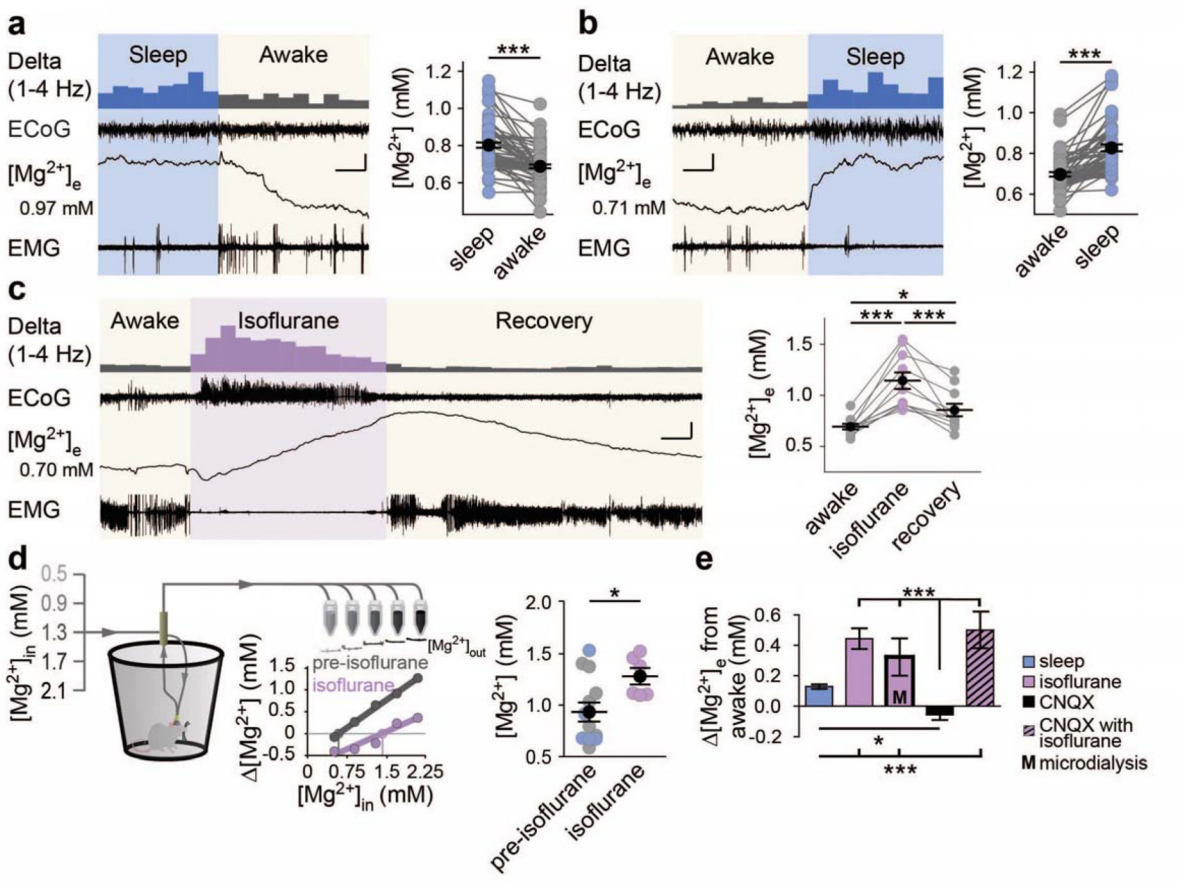

Fig. 4.

Extracellular Mg^{2+} decreases during wakefulness. (**A** and **B**) Representative state-transitions between sleep and awake ECoG, EMG, and Mg^{2+}-sensitive microelectrodes with data summary. Initial $[Mg^{2+}]_e$ is given to the left of the ISM trace. $n = 73$ sleep to awake transitions (**A**) and 58 awake to sleep transitions (**B**). One-way ANOVA: F(3, 258) = 28.13, $P < 0.0001$. Post-hoc Tukey test: $^{***}P < 0.001$. Scale bars: x = 20 s, y = 0.05 mM $[Mg^{2+}]_e$, 0.33 mV EMG/ECoG. (**C**) Representative awake to isoflurane recording (ZT16-20) and summary of changes. $n = 11$ animals. One-way repeated measures ANOVA: F(2,20) = 28.13, $P < 0.0001$. Post-hoc Tukey test: $^{*}P < 0.05$, $^{***}P < 0.001$. Scale bar: x = 5 minutes, y = 0.25 mM $[Mg^{2+}]_e$, 0.6 mV EMG/ECoG. (**D**) Schematic of microdialysis collection with data summary. Representative Mg^{2+}-ISM and no-net flux calculation are shown. Sleep (light blue) and awake (gray) are pooled and compared to isoflurane. n = 8 awake, 8 sleep, and 8 isoflurane. Two-tailed t-test of isoflurane versus pre-isoflurane: $t(16) = 2.427$, $P = 0.0274$. ($^{*}P < 0.05$). (**E**) Comparison of state-dependent $[Mg^{2+}]_e$ shifts from *awake* to sleep, isoflurane, CNQX and awake + CNQX to isoflurane + CNQX. $n =$ awake to CNQX: 6 animals; awake + CNQX to isoflurane + CNQX: 6 animals. One-way ANOVA of relative state-dependent shifts: F(4,167) = 27.31, $P < 0.0001$. Post-hoc Tukey test: $^{**}P < 0.01$, $^{***}P < 0.001$. Mean (black circle) ± SEM.

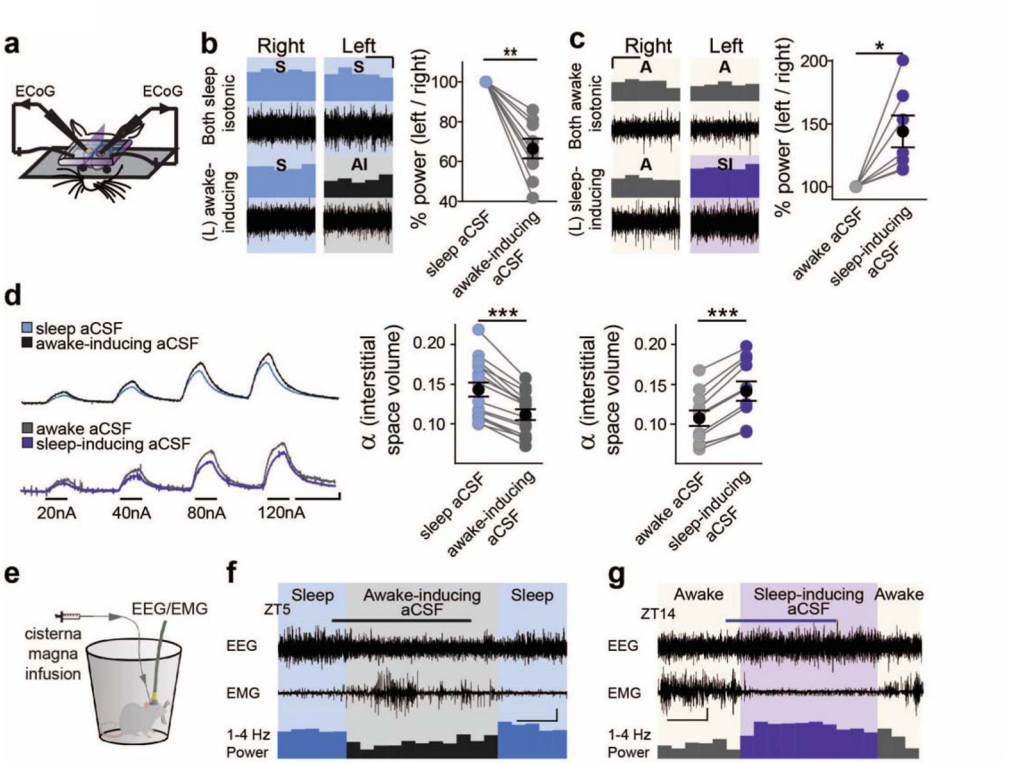

Fig. 5.

Imposing changes in extracellular ion concentrations alter local activity, extracellular space, and behavioral state. (**A**) Schematic of double-cranial window recording setup. Symmetrically positioned, separate cranial windows over opposing somatosensory cortices were prepared with ECoGs simultaneously recorded in both hemispheres. (**B** and **C**) Representative ECoG recordings in **B** sleeping (ZT4-8), and **C** awake (ZT16-20) mice. (*top*) Representative recordings in aCSF mimicking natural state-dependent interstitial ion composition. (*bottom*) Recordings following change of left hemisphere aCSF to awake-inducing (**B**) or sleep-inducing aCSF (**C**) (*right*) Summary of 1–4 Hz ECoG power shift in the left hemisphere, normalized to the right, following change to awake-inducing (**B**) or sleep-inducing (**C**) aCSF. (paired t-test of 1–4 Hz power shifts: **A**: $t(8) = 3.530$, $P = 0.008$; **B**: $t(6) = 3.091$, $P = 0.0214$)). *$P < 0.05$, **$P < 0.01$. Scale bar: x = 4 min, y = 10% (**D**) TMA^+ traces of shifts in extracellular space volume (α) following switch from sleep to awake-inducing aCSF (*upper trace*) or awake to sleep-inducing aCSF (*lower trace*) Note: higher amplitude = decreased dilution of TMA^+, and smaller extracellular space. Data are summarized to the right. Paired t-test (**awake-inducing**: $n = 16$ animals; $t(15) = 11.04$, $P < 0.0001$; **sleep-inducing**: $n = 11$ animals; $t(10) = 8.95$, $P < 0.0001$) **$P < 0.01$. Scale: x = 2 min, y = 2 mV. (**E**) Schematic of cisterna-magna infusion and wire EEG/EMG recording setup. (**F** and **G**) Representative traces showing EEG and EMG activity prior, during, and following a 0.3–0.5 μl min^{-1} infusion of modified awake-inducing (**F**) or sleep-inducing (**G**) aCSF into the cisterna magna. The 1–4 Hz relative power (% of 1–32 Hz) is presented in averaged 10 min bins below. Infusion was run between ZT 5.5-7 (gray bar) (**F**) and

ZT15-16.5 (purple bar) (**G**), during sleep and awake periods, respectively. Scale bar: x = 30 min, y = 0.5 mV (**F**), 1mV (**G**).